Unmarked External Breathing Motion Tracking Based on B-spline Elastic Registration

Huixian Peng[1,2], Lei Deng[1], Zeyang Xia[1], Yaoqin Xie[1], and Jing Xiong[1(✉)]

[1] Shenzhen Institute of Advanced Technology, Chinese Academy of Sciences, Shenzhen 518055, China
jing.xiong@siat.ac.cn

[2] School of Mechatronic Engineering and Automation, Foshan University, Foshan 528255, China

Abstract. In robotic radiosurgery, tracking and modeling of breathing motion is crucial for accurate treatment planning while dealing with tumor inside the thoracic or abdominal cavity, because patient respiration can induce considerable external and internal motion in the thoracic and abdominal regions. Currently, methods for characterizing respiration motion mainly focused on sparse point markers placed on the surface of chest. However, limited number of markers failed to encode the comprehensive features of respiratory motion. Besides, the markers can make partial occlusion during the operation. In this work, a novel method for respiratory motion characterization based on RGB-D camera and B-spline elastic registration is proposed. Images taken from depth camera are used for modeling of abdomen surface during respiration, while B-spline elastic registration technique is applied to restrain the measuring area into an anatomically consistent region during the treatment. In addition, an elastic dynamic motion simulator is designed to test our proposed method. Finally, the feasibility of the method and the device is verified by error analysis and shape comparison.

Keywords: Respiratory motion · B-spline elastic registration · RGB-D camera · Surface modeling

1 Introduction

Radiotherapy is widely used in cancer treatment, because of its constantly improved precision. However, in the process of radiotherapy, there are still remaining uncertain factors resulting in unexpected treatment errors. In the chest and abdomen radiotherapy, the anatomical movement and deformation

Supported by National Natural Science Foundation of China (62073309, 61773365, U2013205 and 61811540033), and Shenzhen Science and Technology Program (JCYJ20200109114812361).

X.-J. Liu et al. (Eds.): ICIRA 2021, LNAI 13015, pp. 71–81, 2021.
https://doi.org/10.1007/978-3-030-89134-3_7

caused by respiratory movement will largely affect the normal implementation of radiotherapy plan [10]. Because of respiration, tumors in abdominal and chest can move nearly 35 mm [3]. Thus, the accurate tacking of treatment target is essential for correctly adjusting the radiation beam in accordance with the target motion to ensure high-precision radiotherapy.

Several traditional methods, such as breath holding, respiratory gating [9,11] and forced shallow breathing with abdominal compression [6], were used to deal with respiratory motion. However, these techniques have some limitations and defects, such as long intervention time, short operative treatment time, and patients' discomfort. Therefore, the real-time tumor tracking methods have raised increased interests, one of those is mainly based on modeling the relationship between internal target and skin surface displacement. Normally, devices are applied to measure the respiratory motion of the skin surface in real-time, which connects a physical device to a patient like marker placed on the patient's surface or an apparatus worn by the patient. For example, the CyberKnife treatment system used three laser sources to record the motion of skin surface in its respiratory tracking system; Ernst et al. [4] proposed a method wherein a shirt with multiple printed markers tracks the respiratory motion using the Kinect v2 device. Alnowami et al. proposed a probability density estimation method, and employed the Codamotion infrared marker-based tracking system to acquire the chest wall motion [1,2]. Wijenayake et al. used stereo cameras to calculate the three-dimensional coordinates of markers, and proposed a motion estimation method based on coded visual markers to predict respiratory motion [12]. However, due to insufficient information of respiratory signals by a limited number of IR markers, there is inevitable accumulation error of targeting in the abdominal region. Moreover, the placement of marker points will block part of the treatment area.

In this paper, a breathing motion modeling system based on commercial RGB-D camera is proposed, which is adapted to trace and record a patient's breathing pattern in a marker-less way. To test the proposed workflow, a respiratory motion simulator is designed. By controlling the patient-specific input signals, the device can simulate the human abdominal breathing motion via motor driven elastic surface deformation so that the anthropomorphic breathing motion can be obtained from the device. First, a certain number of markers are employed to enhance the precision of depth information collection for the RGB-D camera, but these markers are only needed in the process of modeling. After the model is established, it can track any area of the abdomen without markers. Next, the data is analyzed to obtain the images that represent the peak and trough periods of respiration. Finally, the overall motion in the abdomen is modeled by a free-form deformation (FFD) based on B-splines [5,7,8]. The motion of the abdomen during the non-respiratory peak and trough is described by interpolation method.

2 Design of Abdominal Breathing Simulator

2.1 Structure Design

The abdominal breathing simulator, consisting of a driving device, an acrylic box, four sponges and a piece of latex film with markers on its surface, is developed for the simulation of abdominal motion caused by respiration (Fig. 1a). The driving device is an independently controlled vertical platform build in CIRS Dynamic Thorax Simulator (Fig. 1b), which can be programmed by CIRS motion control software to move up and down. However, the device can only move rigidly and simulating the breathing motion of a certain point on the abdominal surface. In order to characterize the breathing motion of the entire abdomen surface, an elastic covering is added, which is supported by an acrylic box with size close to the adult abdomen. The height of the acrylic box will be lower than the lowest height of the driving platform (Fig. 1c). So that fix four sponges with a thickness of 1mm between the driving platform and the latex film can be fixed, where the number of sponges can be added or subtracted according to the shape of human abdomen.

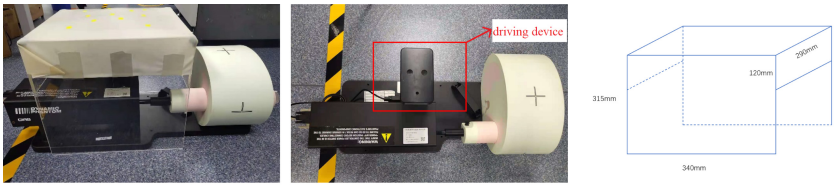

(a) (b) (c)

Fig. 1. (a) Abdominal breathing simulator; (b) Driver device; (c) Dimensions of acrylic box.

2.2 Motion Control

For the dynamic breathing simulation, after importing the patient-specific breathing curve into the CIRS motion control software, the driving device can control the vertical platform motion accurately enough to ensure the real displacement is closely the same with the programmed. When carrying extra load i.e. the tension induced by the deformation of the elastic film, the control accuracy is barely affected according to the former verification experiments. Also, the platform can exert force on the sponge and latex film above, causing the deformation of the sponge and latex film, which visually mimic the morphological states of human abdomen. The overall motion amplitude and period can be easily adjusted by the control software. Although only the convex only shape with single peak can be created, the phantom design was successful because it catches the main motion feature of the abdomen surface under breathing motion. As shown in the Figure, Fig. 2a and Fig. 2b respectively simulate the abdominal state of a real person during inspiration and expiration.

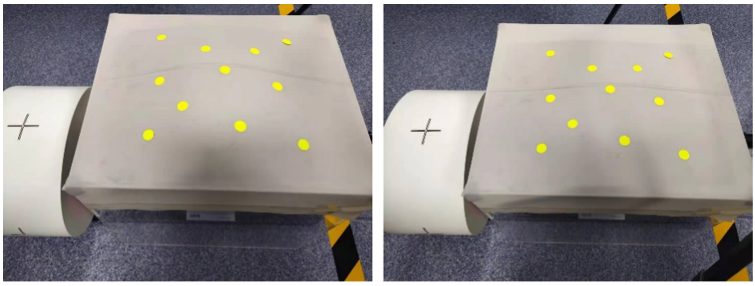

(a) (b)

Fig. 2. (a) Simulate the abdominal state during inspiratory process; (b) Simulate the abdominal state during expiratory process.

3 Design of Tracking Method

3.1 Image Preprocessing

In this paper, a statistical model is constructed based on the motion data of markers representing abdominal motion under respiratory motion. First, the depth image and the corresponding RGB image of the abdomen area are obtained. Then K-nearest neighbor method is applied to fill the gap in the depth image, and then S-G (Savitzky-Golay) filter is used to denoise the depth image. All marks are localized via processing the RGB image. Global binary threshold algorithm (Otsu's method) followed by contour detection and ellipse fitting is applied to identify the center coordinates of each marker accurately in each frame. Corresponding depth value in the depth image are also recorded. The markers are used to track the motion associated with a specific location on the body and monitor the depth change as it moves across the frame.

3.2 Tracking Method

The motion data of markers are averaged and smoothed, to obtain a curve that can represent the abdominal motion frequency under respiratory motion. Then, the number of frames corresponding to the curve in the rising phase and the falling phase of each cycle are counted and averaged. Accordingly, two categories of RGB images belonging to the peak or valley phase are sorted out and unified into two gray level images by frame-wise and channel-wise averaging, during which the abnormal breathing cycle are excluded as outliers. Thus, two feature images that represents the whole abdominal motion during human inhalation and exhalation is acquired.

After obtaining the required gray image, the deformable registration method based on B-spline is applied to make a respiratory motion model. Because, the abdominal motion is nonrigid in general, elastic image registration is necessary

for modeling the dense motion vector fields. The optimal transformation facilitates mapping any point in the dynamic image sequence at one time into its corresponding point in the reference image accurately.

The basic idea of FFD is to deform an object by manipulating an underlying mesh of control points. The resulting deformation controls the shape of the 3-D object and produces a smooth and continuous transformation. Based on the B-spline FFD model, the coordinates of each pixel in the image after moving are calculated, and decompose the movement of the pixels in the image into X and Y directions, then locate the X and Y coordinates respectively.

For any pixel (x, y), the coordinate position (relative to the pixel grid) after cubic B-splines elastic deformation can be expressed as

$$T(x,y) = \sum_{l=0}^{3} \sum_{m=0}^{3} B_l(u) B_m(v) \phi_{i+l,j+m}, \tag{1}$$

where $i = \lfloor x/n_x \rfloor - 1, j = \lfloor y/n_y \rfloor - 1, u = x/n_x - \lfloor x/n_x \rfloor, v = y/n_y - \lfloor y/n_y \rfloor$, and B_l represents the lth basis function of the B-spline

$$\begin{cases} B_0(u) = (1-u)^3/6 \\ B_1(u) = (3u^3 - 6u^2 + 4)/6 \\ B_2(u) = (-3u^3 + 3u^2 + 3u + 1)/6 \\ B_3(u) = u^3/6 \end{cases} \tag{2}$$

The control points act as parameters of the B-spline FFD and the degree of nonrigid deformation which can be modeled depends essentially on the resolution of the mesh of control points. The Φ is used to represent the grid composed of $n_x \times n_y$ control points $\phi_{i,j}(0 \le j < n_x, 0 \le j < n_y)$, and the spacing between each control point is δ.

According to Eq. (1), the optimal solution is obtained ϕ. The main idea is to search for the minimum space transformation position of similarity measure E_{ssd}, which is denoted as

$$E_{ssd} = \frac{1}{N} \sum (I_1(T(x,y)) - I_2(x,y))^2, \tag{3}$$

where N is the total number of pixels in the image registration area, I_1 and I_2 represent the gray function of the reference image and the image to be registered in the two-dimensional space. When these two images match the best, the metric value E_{ssd} reaches minimum.

3.3 Model Optimization

Because the respiratory motion is not strictly periodic, there will be some abnormalities. In order to increase the robustness of the model to deal with the abnormal case, an adaptive link in the model is added. Through the analysis of historical waveform data, the abnormal situation is divided into two cases:

low peak and high valley, for which two models are established. The discrimination of anomalies is out of an empirical criterion. In the case of RGB-D camera tracking anatomic points in real-time, by analyzing the depth information of the initial position of anatomic points, the model can get the index of frames corresponding to the two abnormal situations, and then switch the corresponding model. This method has strengths compared with previous models, which is model parameters trained adaptively by inputting the corresponding images in all abnormal cases. In addition, for improving the tracking accuracy of the model, a self-calibration link in the model is added. The calibration system is modeled as follows:

$$F_{t+1} = (Z_t - F_t) + f_{t+1}, \tag{4}$$

where F_{t+1} and f_{t+1} denote the position frames corresponding to the peaks or valleys output by the model and the uncorrected model at time $t+1$, respectively. And Z_t represents the position frames corresponding to the peaks or valleys output by the initial position of the anatomical point collected by the camera at time t.

4 Experiments and Results

4.1 Data Acquisition

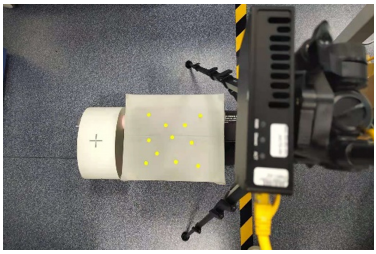

Fig. 3. RGB-D camera is placed nearly 73 cm above the breathing simulation. (Color figure online)

The technology is mainly based on real-time data acquisition by the depth camera (PERCOPIO FM851-GI-E1). The system is designed to track specific pixels from the depth image and record the depth values over time. During the laboratory level experiments, the abdominal breathing simulator is used as the object of data acquisition, 11 yellow non-reflective markers are randomly attached on the surface of the abdomen, and the RGB-D camera is placed nearly 73 cm above the abdomen, as shown in Fig. 3. The number of markers can be greater than or less than 11. Increasing in marker numbers improves amount of acquired abdominal motion information but aggravates the computational burden at the same

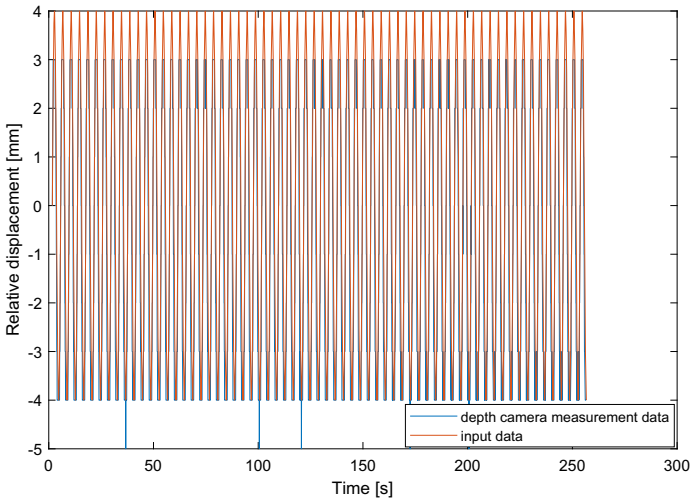

Fig. 4. Experimental results of RGB-D camera accuracy evaluation.

time. The optimum number of markers can balance the modal accuracy and the amount of calculation. Then, the image is acquired and processed according to the method in Sect. 3.1 to acquire the motion data of 11 markers. The data is only used for model building and testing. After the model is built, no markers are needed in the tracking phase.

4.2 Camera Error Test

The motion accuracy of the driving platform in Fig. 2 is ±0.1 mm, so the platform can be used to evaluate the stability and measurement accuracy of the depth camera. Input signal to CRIS control platform is a sinusoidal curve with amplitude as ±4 mm, period as 4 s. At the same time, the motion distance of the platform is measured by using a depth camera. The experimental results are shown in Fig. 4, in which the measurement error of the camera is about 1 mm. In the nearly four minutes of the measurement, the data curve measured by the camera does not appear abnormal fluctuations, indicating that the camera has a good stability.

4.3 Abdominal Breathing Simulator Test

To verify the usefulness of the abdominal breathing simulator. First, the simulated abdominal surface is visualized to observe the shape. As shown in Fig. 5, the device simulates three states of the human body: inhalation, the transition from inspiration exhalation, breathing to inspiration, and exhalation. It can be intuitively observed from the figure that the changes in the volume and area of

the abdomen simulated in the three states are mimic to that of human. Secondly, the depth values of 11 pixels in a period are extracted from the simulated abdominal surface. Figure 6 shows that the change of the depth values of the extracted points shows high correlation with patient breathing motion pattern. Finally, the data of the human abdominal surface in two states of inspiration and respiration are extracted. In Fig. 7, compared with the inspiratory and expiratory states simulated by the abdominal breathing simulator, the morphological changes of the two states are very close. Thus, the usefulness and feasibility of the abdominal breathing simulation device proposed in this paper are illustrated.

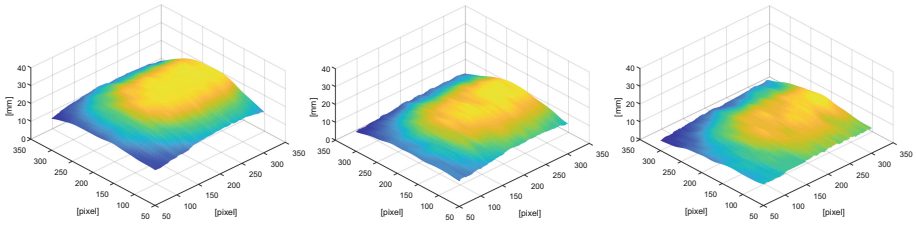

Fig. 5. The device simulates three states of the human body: (a) inhalation, (b) transition between inhalation and exhalation, (c) exhalation.

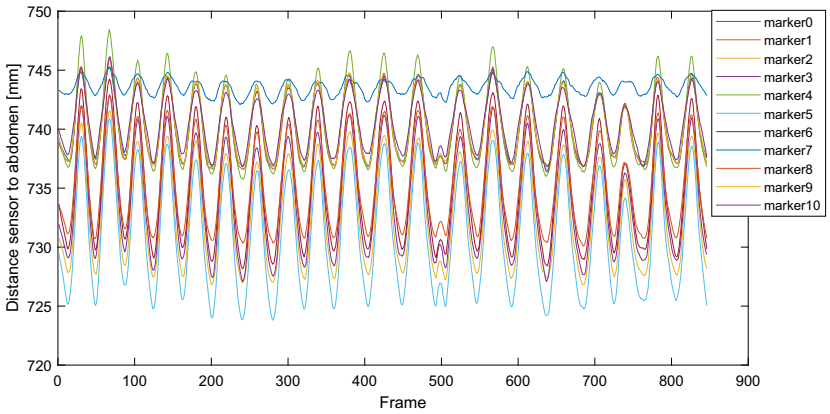

Fig. 6. The depth values of 11 pixels in a period of time.

4.4 Model Method Validation

To make the quantitative comparison, 11 markers randomly distributed on the surface of the abdomen are selected. The center coordinates of each point mark

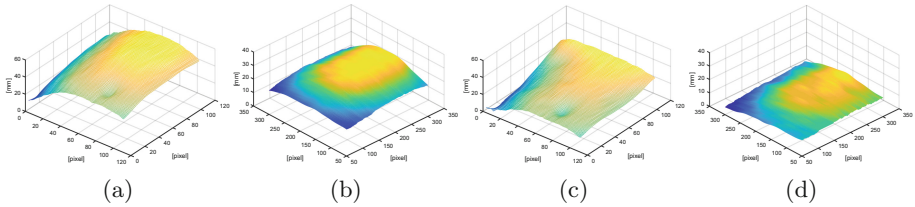

Fig. 7. Comparison of the shape of abdominal breathing simulator and human in the state of inspiration and expiration.

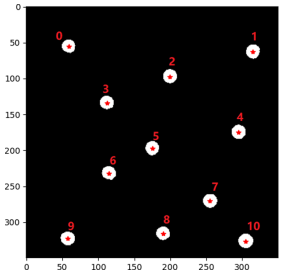

Fig. 8. Center positioning result of marker.

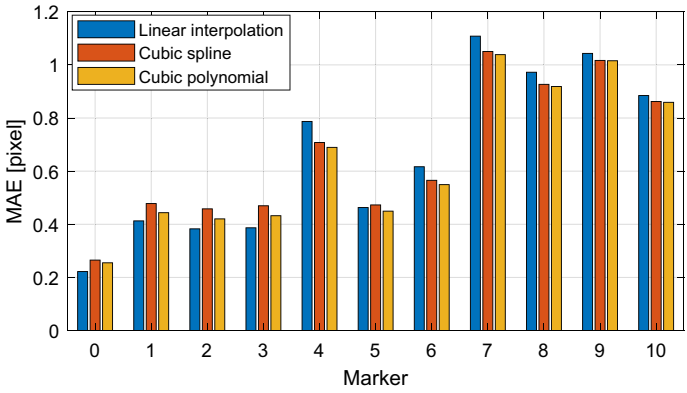

Fig. 9. Histogram of mean absolute error (MAE) of three interpolation methods.

are accurately determined in each frame (Fig. 8), and the relative displacement data of 11 markers on the abdominal surface during a period of breathing motion are obtained. The tracking error of the model is also evaluated based on the data measured by the image segmentation method. Equation 5 is used to calculate the motion error.

$$MAE = \frac{1}{N}\sum_{i=1}^{n}\left|\sqrt{x_i^2 + y_i^2} - \sqrt{X_i^2 + Y_i^2}\right| \tag{5}$$

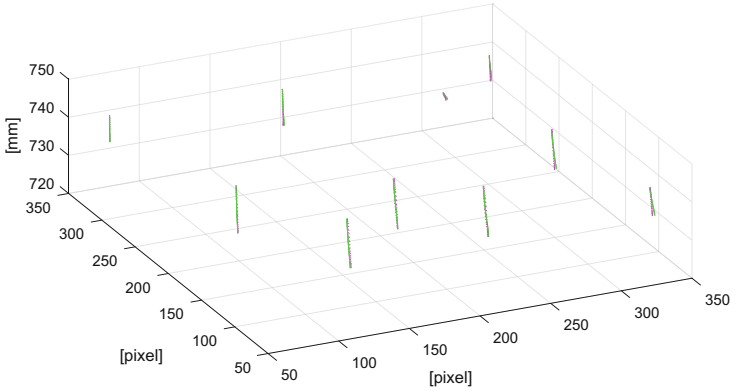

Fig. 10. Trajectory of all markers. The purple dotted line represents the predicted marker trajectory, and the green dotted line represents the real marker trajectory. (Color figure online)

The (X_i, Y_i) represents the coordinates of the markers in i^{th} frame, and (x_i, y_i) denotes the marker coordinates predicted by the model in i^{th} frame.

Linear interpolation, cubic spline interpolation, and cubic polynomial interpolation are separately used in the model. The motion errors calculated by the three interpolation methods are shown in Fig. 9. As can be seen from Fig. 9, except that the average absolute error of marker 7 and marker 9 is more than one pixel, the error of other mark points is less than one pixel. For marked points 4∼10, the error of the cubic polynomial interpolation method is lower than the other two interpolation methods. For the marked points 0∼3, the error of linear interpolation is lower and the results improved. In general, the cubic polynomial interpolation outperforms the others with the manually fine-tuned parameters.

Finally, in order to see the tracking effect more intuitively, this paper visualizes all the marked tracking curves. As shown in Fig. 10, The purple dotted line represents the predicted marker trajectory, and the green dotted line represents the real marker trajectory. The purple dotted line tracks the motion trend that complies well with the green dotted line, which shows the feasibility and accuracy of the proposed model.

5 Conclusion

In this study, a non-contact, non-invasive, and real-time breathing motion measurement technology is introduced. During the real-time tracking, the model does not require any markers or other devices on the human abdominal surface. Compared with the previous methods of tracking the abdominal target area using limited markers, our method of state-to-state image registration can achieve better results. In addition, through the accurate tracking verification of multiple marked points on the abdomen, this paper realizes the tracking from multiple

points to surface, which can predict the position of any point on the abdominal surface. In future, in order to improve the tracking accuracy, we will further optimize the model by increasing the adaptability of the model. At the same time, we will optimize the representation method of abdominal surface state, and strive to provide more abundant and accurate information for respiratory tracking of radiosurgery robots.

References

1. Alnowam, M.R., Lewis, E., Wells, K., Guy, M.: Respiratory motion modelling and prediction using probability density estimation. In: IEEE Nuclear Science Symposium & Medical Imaging Conference, pp. 2465–2469. IEEE (2010)
2. Alnowami, M., Lewis, E., Wells, K., Guy, M.: Inter-and intra-subject variation of abdominal vs. thoracic respiratory motion using kernel density estimation. In: IEEE Nuclear Science Symposium & Medical Imaging Conference, pp. 2921–2924. IEEE (2010)
3. Barnes, E.A., Murray, B.R., Robinson, D.M., Underwood, L.J., Hanson, J., Roa, W.H.: Dosimetric evaluation of lung tumor immobilization using breath hold at deep inspiration. Int. J. Radiat. Oncol.* Biol.* Phys. **50**(4), 1091–1098 (2001)
4. Ernst, F., Saß, P.: Respiratory motion tracking using Microsoft's Kinect V2 camera. Curr. Dir. Biomed. Eng. **1**(1), 192–195 (2015)
5. Holden, M.: A review of geometric transformations for nonrigid body registration. IEEE Trans. Med. Imaging **27**(1), 111–128 (2007)
6. Keall, P.J., et al.: The management of respiratory motion in radiation oncology report of AAPM task group 76 a. Med. Phys. **33**(10), 3874–3900 (2006)
7. Lee, S., Wolberg, G., Chwa, K.Y., Shin, S.Y.: Image metamorphosis with scattered feature constraints. IEEE Trans. Vis. Comput. Graph. **2**(4), 337–354 (1996)
8. Lee, S., Wolberg, G., Shin, S.Y.: Scattered data interpolation with multilevel b-splines. IEEE Trans. Vis. Comput. Graph. **3**(3), 228–244 (1997)
9. Mageras, G.S., et al.: Fluoroscopic evaluation of diaphragmatic motion reduction with a respiratory gated radiotherapy system. J. Appl. Clin. Med. Phys. **2**(4), 191–200 (2001)
10. Ozhasoglu, C., Murphy, M.J.: Issues in respiratory motion compensation during external-beam radiotherapy. Int. J. Radiat. Oncol.* Biol.* Phys. **52**(5), 1389–1399 (2002)
11. Vedam, S., Keall, P., Kini, V., Mohan, R.: Determining parameters for respiration-gated radiotherapy. Med. Phys. **28**(10), 2139–2146 (2001)
12. Wijenayake, U., Park, S.Y.: Respiratory motion estimation using visual coded markers for radiotherapy. In: Proceedings of the 29th Annual ACM Symposium on Applied Computing, pp. 1751–1752 (2014)